

Article

# Determination of Interface-State Distributions in Polymer-Based Metal-Insulator-Semiconductor Capacitors by Impedance Spectroscopy

Hideyuki Hatta <sup>1</sup>, Yuhi Miyagawa <sup>1</sup>, Takashi Nagase <sup>1,2,\*</sup> , Takashi Kobayashi <sup>1,2</sup>,  
Takashi Hamada <sup>1,†</sup>, Shuichi Murakami <sup>3</sup> , Kimihiro Matsukawa <sup>4</sup> and Hiroyoshi Naito <sup>1,2,\*</sup> 

<sup>1</sup> Department of Physics and Electronics, Osaka Prefecture University, 1-1 Gakuen-cho, Naka-ku, Sakai 599-8531, Japan; hide.hatta@gmail.com (H.H.); miyagawa.pe3@gmail.com (Y.M.); tkobaya@pe.osakafu-u.ac.jp (T.K.); hamada.takashi@qst.go.jp (T.H.)

<sup>2</sup> The Research Institute for Molecular Electronic Devices, Osaka Prefecture University, 1-1 Gakuen-cho, Naka-ku, Sakai 599-8531, Japan

<sup>3</sup> Osaka Research Institute of Industrial Science and Technology, 2-7-1 Ayumino, Izumi, Osaka 594-1157, Japan; sh-murakami@tri-osaka.jp

<sup>4</sup> Kyoto Institute of Technology, Matsugasaki, Sakyo-ku, Kyoto 606-8585, Japan; kmatsu@kit.ac.jp

\* Correspondence: nagase@pe.osakafu-u.ac.jp (T.N.); naito@pe.osakafu-u.ac.jp (H.N.); Tel.: +81-72-254-9266 (H.N.)

† Present address: Department of Advanced Functional Materials Research, Takasaki Advanced Radiation Research Institute, Quantum Beam Science Research Directorate, National Institutes for Quantum and Radiological Science and Technology, 1233 Watanuki, Takasaki, Gunma 370-1292, Japan.

Received: 3 August 2018; Accepted: 21 August 2018; Published: 29 August 2018



**Abstract:** Information on localized states at the interfaces of solution-processed organic semiconductors and polymer gate insulators is critical to the development of printable organic field-effect transistors (OFETs) with good electrical performance. This paper reports on the use of impedance spectroscopy to determine the energy distribution of the density of interface states in organic metal-insulator-semiconductor (MIS) capacitors based on poly(3-hexylthiophene) (P3HT) with three different polymer gate insulators, including polyimide, poly(4-vinylphenol), and poly(methylsilsesquioxane). The findings of the study indicate that the impedance characteristics of the P3HT MIS capacitors are strongly affected by patterning and thermal annealing of the organic semiconductor films. To extract the interface-state distributions from the conductance of the P3HT MIS capacitors, an equivalent circuit model with continuum trap states is used, which also takes the band-bending fluctuations into consideration. In addition, the relationship between the determined interface states and the electrical characteristics of P3HT-based OFETs is investigated.

**Keywords:** organic metal-insulator-semiconductor capacitor; organic field-effect transistor; polymer gate insulator; interface states; impedance spectroscopy

## 1. Introduction

In recent years, the development of solution-processable organic field-effect transistors (OFETs) has attracted increasing interest owing to their widespread use in various printable electronic devices, including flexible displays, low-cost radio-frequency identification tags, and large-area sensors [1,2]. It is well known that carrier transport in OFETs is sensitive to the ordering and packing of the organic semiconducting molecules interfaced with the gate insulator, and localized trap states caused by the disorder significantly affect the electrical performance of OFETs, such as field-effect mobility, threshold voltage, and subthreshold slope. It has been reported that molecular ordering in the

organic semiconductor films of OFETs with bottom-gate configurations, which are conventionally used for OFET applications, depends largely on the surface properties, such as surface energy [3,4] and roughness [5], of the underlying gate insulators. Therefore, the development of reliable organic gate insulators is critical for improving the performance of bottom-gate OFETs. For the development of solution-processable OFETs, thermally curable polymer gate insulators, such as polyimide (PI) [6,7], poly(4-vinylphenol) (PVP) [8], and poly(methylsilsesquioxane) (PMSQ) [9–12], have gained much attention because these materials allow the formation of desirable semiconductor/insulator interfaces with limited interfacial mixing.

The localized trap states at the solution-processed organic semiconductor/polymer gate insulator interfaces have been studied by measuring the impedance characteristics of metal-insulator-semiconductor (MIS) capacitors [13–18]. It has been reported that the impedance characteristics of organic MIS capacitors can be described with equivalent circuit models similar to those of Si-based metal-oxide-semiconductor (MOS) capacitors, which were suggested by Nicollian and Goetzberger [19,20]; further, energetically distributed localized states are formed at the organic semiconductor/polymer gate insulator interfaces [14–16]. However, the influence of the polymer gate insulators on the interface states in organic MIS capacitors has not been ascertained in existing literature.

In this paper, we report the determination of interface-state distributions in poly(3-hexylthiophene) (P3HT)-based organic MIS capacitors with polymer gate insulators of PI, PVP, and PMSQ using impedance spectroscopy (IS). First, we discuss the influences of patterning and thermal annealing of the organic semiconductor films on the impedance characteristics of P3HT MIS capacitors to determine the optimal fabrication process for our tested MIS devices. Next, we examine the applicability of three equivalent circuit models to the extraction of interface states from the conductance characteristics of the P3HT MIS capacitors. Finally, we attempt to identify the correlation between the densities of interface states in the organic MIS capacitors and the electrical characteristics of OFETs.

## 2. Experimental

Figure 1 illustrates the schematic of the fabricated organic MIS capacitor, along with the chemical structures of organic materials used in this study. Striped indium tin oxide (ITO) electrodes with a 3 mm width formed on a slide glass were used as the gate electrodes, and 2 mm-wide gold electrodes were deposited on top of an organic semiconductor layer to fabricate the organic MIS device with crossed top and bottom electrodes. As the gate insulators, thermally-curable polymer insulators, PI (SE-5291, Nissan Chemical Co. (Tokyo, Japan)), PVP (Sigma-Aldrich Co. (St. Louis, MO, USA)) mixed with the cross-linking agent of poly(melamine-co-formaldehyde) (PMF) (the weight ratio of 2.8:1), and PMSQ prepared in our laboratory [10–12], were used.

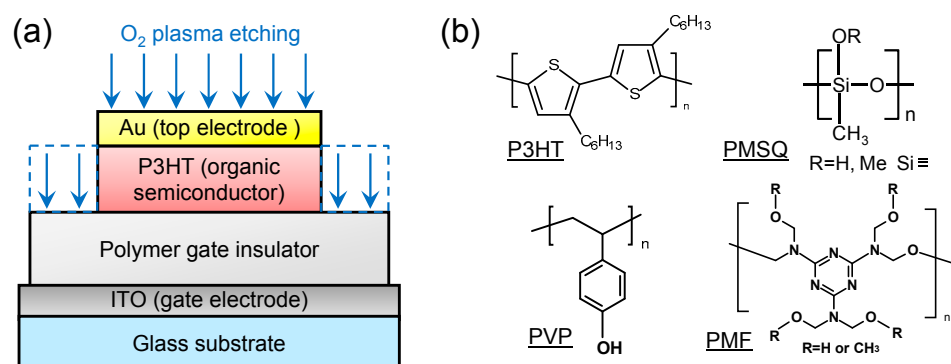


**Figure 1.** (a) Schematic cross section of the organic MIS capacitor after O<sub>2</sub> plasma etching. The dotted squares represent the peripheral regions removed by etching. (b) Chemical structures of organic materials used in this study.

The glass substrates with ITO gate electrodes were cleaned with acetone and isopropyl alcohol (IPA) in an ultrasonic bath and with an UV/O<sub>3</sub> cleaner. Subsequently, the organic solutions of polymer insulators were deposited on the substrates by spin coating, and then the obtained films were thermally cured for 1 h (at 185, 200, and 150 °C for PI, PVP, and PMSQ insulators, respectively) to form polymer gate insulators with thicknesses of ~400 nm on the gate electrodes. The organic semiconductor films with thickness of ~200 nm were fabricated by spin coating a 3 wt% toluene solution of regioregular P3HT ( $M_n = 45,000\text{--}65,000$ , Sigma-Aldrich Co.) on the polymer gate insulators. Then, Au top electrodes were fabricated on P3HT films by shadow mask evaporation. Finally, the P3HT films on the gate insulators were patterned using O<sub>2</sub> plasma etching (Samco RIE10-N (Kyoto, Japan)) using Au top electrodes as etching masks. The O<sub>2</sub> plasma generated at a pressure of 250 mTorr, a flow rate of 45 sccm, and a radio-frequency power of 120 W was irradiated for 5 min to remove the P3HT films not coated by the Au top electrodes (the peripheral region of the organic MIS capacitors). We also fabricated the MIS capacitors without patterning the P3HT films to investigate the influence of the peripheral region on the impedance characteristics of the organic MIS capacitors.

The fabricated P3HT MIS capacitors were annealed in a vacuum chamber at 90–100 °C over 3 h to remove adventitious dopants, such as O<sub>2</sub> and H<sub>2</sub>O, from the P3HT films, and the impedance characteristics of the P3HT MIS capacitors were measured in the vacuum chamber at room temperature without breaking the vacuum to avoid doping to the P3HT films by ambient air. Impedance measurements were carried out using a Solartron 1260 impedance analyzer with a 1296 dielectric interface (Farnborough, Hampshire, UK), and sinusoidal signals with a 100-mV amplitude and frequencies ranging from 0.1 Hz to 1 MHz were superimposed on the gate voltage ( $V_G$ ). The electrical characteristics of the P3HT-based OFETs with polymer gate insulators were measured using Keithley 6430 and 2400 source meters (Cleveland, OH, USA) in a glove box filled with N<sub>2</sub>. All electrical measurements were performed in a dark environment to prevent the influence of photocarrier generation on the electrical characteristics of the organic MIS devices [21].

### 3. Results and Discussion

#### 3.1. Optimization of the Fabrication Processes of Organic MIS Capacitors

First, we describe the influence of the patterning of organic semiconductor films in the P3HT MIS capacitors with crossed top and bottom electrodes on their impedance characteristics. Figure 2a shows the capacitance–frequency characteristics of the MIS capacitor with the P3HT film patterned using O<sub>2</sub> plasma etching. The MIS capacitor with the patterned P3HT film exhibits reasonable dependencies on frequency and gate voltage. In an ideal MIS diode with a *p*-type organic semiconductor, when the gate electrode is negatively biased, holes are injected from the top electrode and accumulate at the interface between the semiconductor and the gate insulator. This leads to the increase in the capacitance of the MIS capacitor, which approaches the capacitance of the gate insulator ( $C_i$ ) when the frequency of the sinusoidal signal is extremely low because holes accumulate in the whole area of the semiconductor/gate insulator interface. At high frequencies, the injected holes do not follow the sinusoidal signal, leading to the depletion of the organic semiconductor film, which reduces the capacitance of the MIS capacitor. When the organic semiconductor films are completely depleted, the capacitance of the MIS capacitor ( $C$ ) can be expressed by the series sum of a capacitance of semiconductor film ( $C_S$ ) and  $C_i$ ;  $C = C_S C_i / (C_S + C_i)$ .

The capacitance–frequency characteristics of the MIS capacitor fabricated without patterning P3HT film are shown in Figure 2b. The capacitance of the MIS capacitor with the unpatterned P3HT film increases with decreasing frequency, indicating an excess accumulation of holes at the semiconductor/gate insulator interface. It has been reported that holes injected from the top electrodes spread laterally across the semiconductor film to form an additional channel; this channel is responsible for the increase in the capacitance of the MIS capacitors in the low frequency regime [22–24]. To suppress such effects associated with lateral conduction along the semiconductor film, a circular

top electrode surrounded by a concentric guard ring has been generally used in Si-based MOS capacitors [22] and organic MIS capacitors [13–16,18,23]. Our experimental results demonstrate that the organic MIS capacitors with crossed top and bottom electrodes can be used for impedance measurements by patterning the organic semiconductor films using O<sub>2</sub> plasma etching.

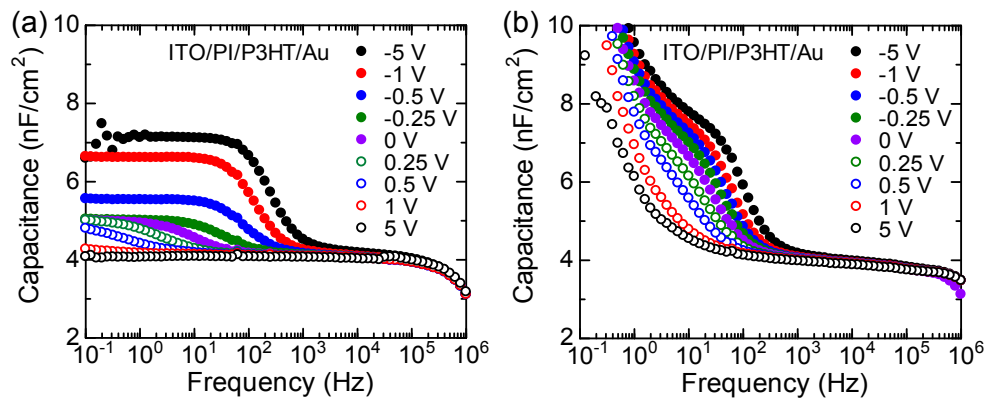


**Figure 2.** Frequency dependences of the capacitance of the ITO/PI/P3HT/Au MIS capacitors with (a) patterned and (b) unpatterned P3HT films measured at various gate voltages.

Figure 3a and b show the frequency dependence of the loss (conductance ( $G$ )/angular frequency ( $\omega$ )) of the organic MIS capacitors with patterned and unpatterned P3HT films, respectively. The conductance was determined by calculating the real part of admittance ( $Y$ ) according to  $Y = G + j\omega C$ . The figures indicate that the peripheral regions of the organic MIS capacitors significantly affect the position and magnitude of loss peaks. In Figure 3a, the peak position shifts to a higher frequency with increasing negative gate voltage. On the other hand, the response of an ideal MIS capacitor in the depletion mode can be described in the equivalent circuit shown in Figure 4a. In the figure,  $C_i$  represents the insulator capacitance,  $C_d$  represents the depletion capacitance,  $C_b'$  and  $R_b'$  represent the capacitance and resistance, respectively, of the bulk semiconductor, and  $R_C$  represents the contact resistance. The relaxation frequency ( $f_R$ ) of the circuit is given by

$$f_R = \frac{1}{2\pi R_b'(C' + C_b')} = \frac{1}{2\pi\tau}, \quad (1)$$

where  $\tau$  is the relaxation time of the MIS capacitor and  $C'$  represents the series sum of  $C_i$  and  $C_d$  [14,15]. According to Equation (1), the relaxation frequency should increase when the positive gate voltage is increased because it leads to an increase in the depletion width and hence decreases in  $C'$ . This feature is contrary to the results shown in Figure 3a, in which the loss peak shifts to the low frequency regime when the positive gate voltage is increased. Such apparent decrease in the relaxation frequency is similar to the behavior of interface states reported for Si-based MOS capacitors [19,20]. Hence, the equivalent circuit of the P3HT MIS capacitor should include an array of series  $RC$  elements ( $R_t, C_t$ ) in parallel with  $C_d$  to account for the observed  $G/\omega-f$  characteristics, as shown in Figure 4b.

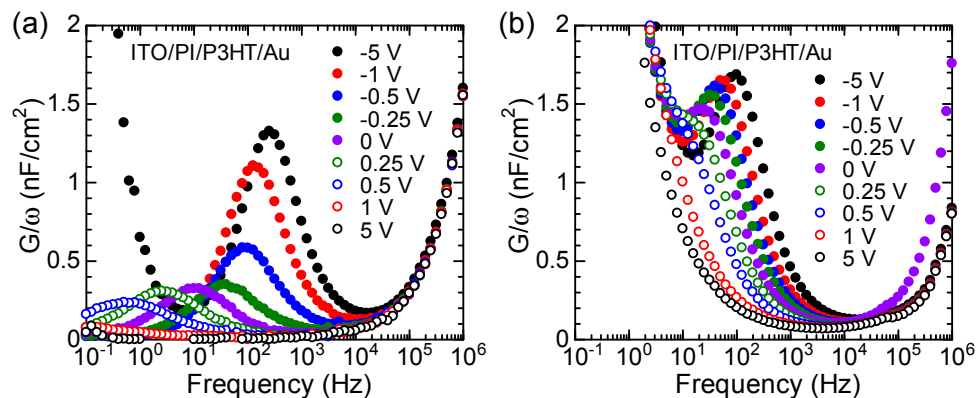


**Figure 3.** Frequency dependences of the conductance loss ( $G/\omega$ ) of the ITO/PI/P3HT/Au MIS capacitors with (a) patterned and (b) unpatterned P3HT films measured at various gate voltages.

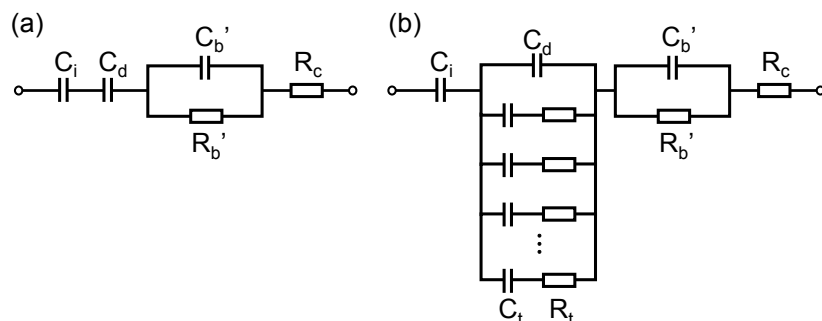


**Figure 4.** (a) Equivalent circuits representing an ideal MIS capacitor and (b) a MIS capacitor with energetically distributed interface states.

Another issue detrimental to the interface states in the organic MIS capacitors is the influence of unintended doping on organic semiconductor films. In particular, the electrical characteristics of P3HT-based OFETs are well known to significantly suffer from hole doping to P3HT films by  $\text{O}_2$  and  $\text{H}_2\text{O}$  in ambient air [25]; further, the density of the interface states in P3HT MIS capacitors was found to depend on the dopant concentration [15]. Therefore, removing the dopants via the thermal annealing process is critical for the accurate determination of interface-state densities from organic MIS capacitors. In this work, we investigated the effect of thermal annealing on the dopant concentration by using capacitance–gate voltage ( $C-V_G$ ) measurements of the P3HT MIS capacitors with PI gate insulator.

Figure 5a shows the variation in the  $C-V_G$  characteristics of the P3HT MIS capacitor measured at 100 Hz before and after thermal annealing. In the experiment, the impedance characteristics of the MIS capacitors were measured at room temperature after thermal annealing at 100 °C for 1 h in a vacuum; this cycle was repeated five times (in the fifth cycle, the device was thoroughly annealed for 5 h). The dopant concentration in the P3HT film can be determined using Schottky–Mott analysis [26] from the slopes of the  $1/C^2-V_G$  curves in the transition region between accumulation and depletion. The dopant concentration ( $N_A$ ) is given as follows,

$$N_A = 2 \left[ q\epsilon_0\epsilon_r A^2 \frac{d}{dV_G} \left( \frac{1}{C^2} \right) \right]^{-1}, \quad (2)$$

where  $q$  is the elementary charge,  $\epsilon_0$  is the permittivity of vacuum,  $\epsilon_r$  is the relative permittivity of the semiconductor, and  $A$  is the active area of the MIS capacitor.

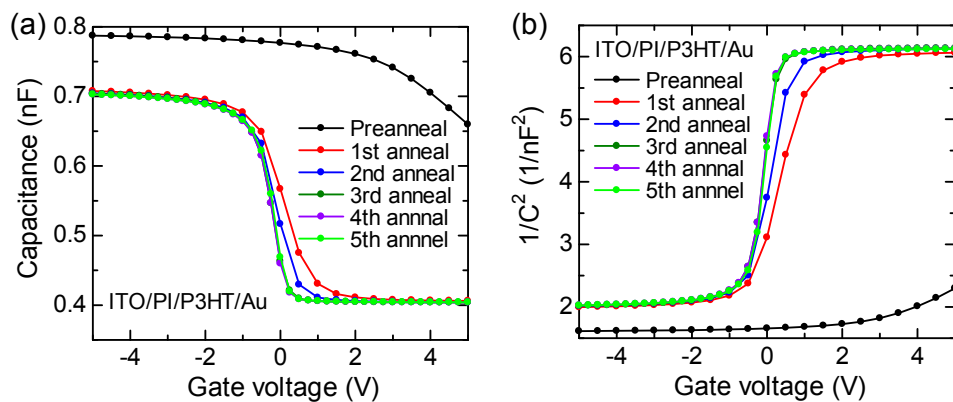


**Figure 5.** (a) Gate voltage dependences of the capacitance ( $C$ ) and (b)  $1/C^2$ -gate voltage plots in the ITO/PI/P3HT/Au MIS capacitor without the peripheral regions measured at 100 Hz after each thermal annealing cycle.

Figure 5b shows  $1/C^2-V_G$  curves plotted from Figure 5a, and Table 1 summarizes the values of the dopant concentration for thermal annealing cycles estimated using Equation (2) by assuming  $\varepsilon_r = 3$ . The dopant concentration decreased dramatically after the first annealing cycle, and remained almost unchanged after the third annealing cycle, indicating that most dopants were removed from the P3HT film. The dopant concentration after the fifth annealing cycle was  $1.4 \times 10^{15} \text{ cm}^{-3}$ , which is much lower than those reported for P3HT MIS capacitors [15,27]. These results suggest that the optimized device fabrication of the organic MIS capacitors enables the investigation of the influence of the gate insulator on the interface-state density via impedance measurements.

**Table 1.** Variation of the dopant concentration ( $N_A$ ) for annealing cycle in the ITO/PI/P3HT/Au MIS capacitor.

Annealing Cycle	$N_A (\text{cm}^{-3})$
Before annealing	$1.6 \times 10^{16}$
1st	$2.8 \times 10^{15}$
2nd	$2.0 \times 10^{15}$
3rd	$1.4 \times 10^{15}$
4th	$1.4 \times 10^{15}$
5th	$1.4 \times 10^{15}$

### 3.2. Determination of the Interface States of MIS Capacitors with Different Polymer Gate Insulators

To investigate the influence of the polymer gate insulator on the interface-state density in P3HT MIS capacitors, we analyzed the impedance characteristics by using the conductance method suggested by Nicollian and Goetzberger [19,20]. In order to extract the interface states from the conductance, three equivalent circuit models that incorporate the interface states with a single energy level, continuum energy levels, and continuum interface states affected by band-bending fluctuations were proposed. Hereafter, we refer to these as the single-level model, the continuum model, and the statistical model, respectively.

Figure 6a illustrates an equivalent circuit of an MIS capacitor that incorporates the interface states with the single energy level in the depletion mode. Here,  $C_t$  and  $G_t$  represent the capacitance and conductance associated with interface states, respectively. The simplified version of Figure 6a is shown in Figure 6b. When the equivalent circuit shown in Figure 6b is converted into that shown in Figure 6c, the equivalent parallel conductance ( $G_p$ ) divided by  $\omega$  (loss) is given by

$$\frac{G_p}{\omega} = \frac{qD_{it}\omega\tau_p}{1 + \omega^2\tau_p^2}, \quad (3)$$

where  $D_{it}$  and  $\tau_p$  are the density of interface states and the time constant of the interface states, respectively. Figure 6d shows an equivalent circuit with the continuum interface states, which is represented by  $G_t - C_t$  branches parallel to the depletion layer. In the case of the continuum model, the loss can be expressed as

$$\frac{G_p}{\omega} = \frac{qD_{it}}{2\omega\tau_p} \ln(1 + \omega^2\tau_p^2). \quad (4)$$

In the statistical model, the influence of built-in charges and/or charged interface states was also assumed [20,28,29]. It is assumed that a random spatial distribution of discrete interface charges results in a spatial distribution of band bending. The probability that the band bending is  $v_s$  is expressed as

$$P(v_s) = (2\pi\sigma_s^2)^{-1/2} \exp\left[-\frac{(v_s - \langle v_s \rangle)^2}{2\sigma_s^2}\right], \quad (5)$$

where  $\sigma_s^2$  is the variance of band bending, expressed in terms of  $kT/q$ , and  $\langle v_s \rangle$  is the mean value of the band bending. In this case, Equation (4) can be rewritten as follows

$$\frac{G_p}{\omega} = \frac{q}{2} \int_{-\infty}^{\infty} \frac{D_{it}}{\omega\tau_p} \ln(1 + \omega^2\tau_p^2) P(v_s) dv_s. \quad (6)$$

From the above expressions, we obtain

$$\frac{G_p}{\omega} = \frac{qD_{it}(2\pi\sigma_s^2)^{-1/2}}{2\omega\tau_p} \int_{-\infty}^{\infty} \exp\left(-\frac{\eta^2}{2\sigma_s^2}\right) \exp(-\eta) \ln(1 + \omega^2\tau_p^2 \exp 2\eta) d\eta, \quad (7)$$

where  $\eta = v_s - \langle v_s \rangle$ . The density of the interface states can be determined by fitting Equations (3), (4), or (7) to the frequency dependence of loss ( $G_p/\omega - f$ ).

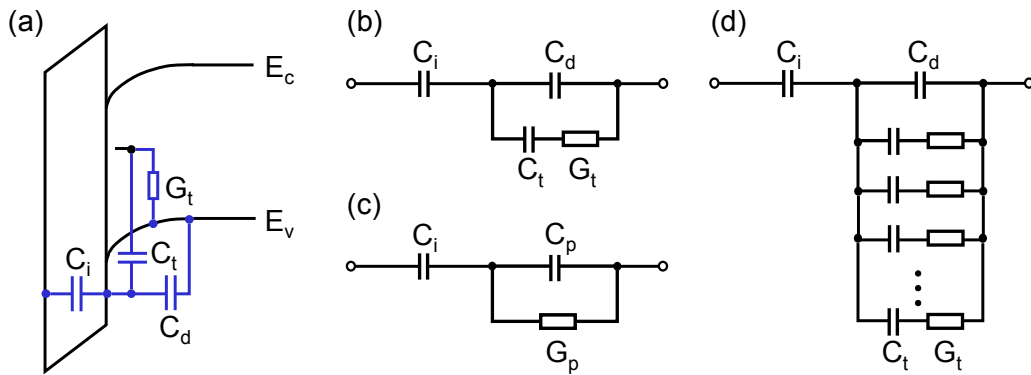


**Figure 6.** (a) Equivalent circuit of a MIS capacitor with single-energy level interface states in depletion mode and (b) simplified version of (a). (c) Lumped parallel equivalent circuit of (b) or (d). (d) Equivalent circuit of a MIS capacitor with energetically distributed interface states.

First, we examined the applicability of the three models for the P3HT MIS capacitors with polymer gate insulators. The  $G_p/\omega - f$  curve of the MIS capacitor with the PI gate insulator extracted from the measured impedance spectrum at a gate voltage of 0 V is shown in Figure 7a, in which the fitted curves using the three models are also indicated. It can be seen that the measured  $G_p/\omega - f$  curve is broader than the calculated curve using Equation (3), indicating that the interface states in the P3HT MIS capacitors are energetically distributed [14–16,18]. Moreover, we found that the statistical model

is in better agreement with the experimental curve than the continuum model. This suggests that the equivalent circuit model, which takes band-bending fluctuations into consideration, is appropriate to describe the impedance characteristics of P3HT MIS capacitors. As shown in Figure 7b, the fitted  $G_p/\omega-f$  curves using the statistical model are in good agreement with the experimental curves obtained for different gate voltages: the energy distributions of interface-state densities can be determined using these curves.

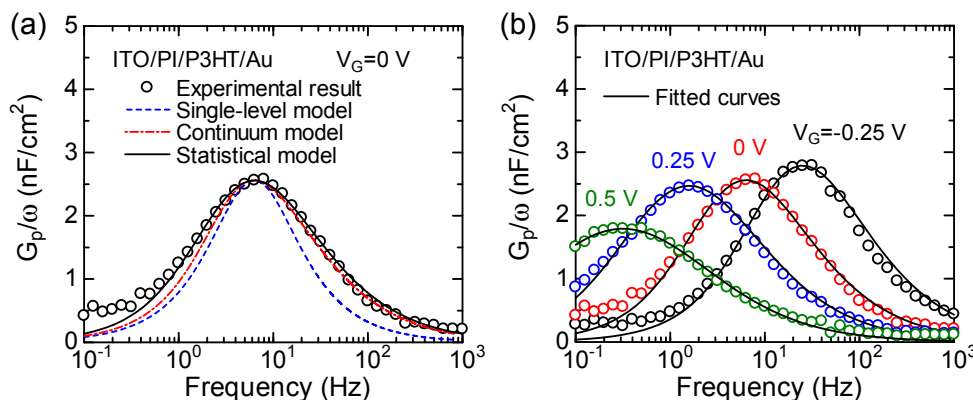


**Figure 7.** (a) Plot of the equivalent parallel conductance loss ( $G_p/\omega$ ) versus frequency for the P3HT MIS capacitor with the PI gate insulator at a gate voltage ( $V_G$ ) of 0 V. The dashed blue line, dashed-dotted red line, and solid black lines represent the fitted results using Equations (3), (4) and (7), respectively. (b) Fitted results for the frequency dependence of  $G_p/\omega$  of the ITO/PI/P3HT/Au MIS capacitor at different gate voltages using the statistical model.

Figure 8 shows the densities of interface states above the valence band edge ( $E_v$ ) in the P3HT MIS capacitors with the different polymer insulators of PI, PVP, and PMSQ, calculated using the statistical model. The energy scale was determined by the conventional C–V method [30]. The energy level was calculated from the surface potential ( $\psi_s$ ) at  $V_G$ , which is given as follows

$$E - E_V = \psi_s(V_G) = \int_{V_{FB}}^{V_G} \left(1 - \frac{C_m}{C_i}\right) dv, \quad (8)$$

where  $C_m$  is the capacitance at low frequency and  $V_{FB}$  is the flatband voltage. The value of  $V_{FB}$  was assumed to be  $-0.5$  V for all samples. In Figure 8, the density of interface states in P3HT MIS capacitors is shown to be strongly affected by the type of polymer gate insulators; the density of interface states for P3HT MIS capacitors with PMSQ insulators is relatively lower than that with other polymer insulators.

To examine the influence of gate insulators on FET characteristics, bottom-gate/top-contact P3HT FETs were fabricated on polymer gate insulators. In the FET devices, thin P3HT films ( $\sim 50$  nm) were used. Their transfer characteristics (drain current ( $I_D$ )– $V_G$ ) are shown in Figure 9; it can be seen that  $I_D$  and the subthreshold slope (SS) largely depend on the type of gate insulators. The field-effect mobilities and SS values of P3HT FETs as well as the water contact angles on polymer insulators are summarized in Table 2. The table clearly illustrates the relationship between mobility, SS value, and the water contact angle. The mobility increases and the SS value decreases as the water contact angle on polymer insulators is increased. Moreover, the mobilities and SS values are closely correlated to the density of interface states shown in Figure 8. It is well known that the SS value is inversely proportional to the total density of interface states [31]. Therefore, based on the obtained results, the improvement in the mobility and SS value can be attributed to the decrease in the interface-state density. The difference in the interface-state densities in the P3HT MIS capacitors with different polymer insulators is attributable to the difference in the surface energy of the gate insulators. It has been reported that the orientation and packing of P3HT molecules are largely dependent on the hydrophobicity of substrates; it has

also been suggested that lower surface energy leads to higher crystallization of P3HT films [3]. Thus, the observed low density of interface states at the P3HT/PMSQ interfaces can be attributed to the improvement in film crystallinity at low-energy surfaces.

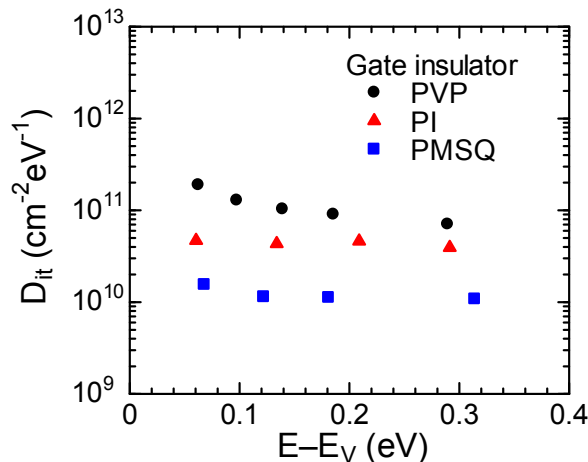


**Figure 8.** Densities of interface states ( $D_{it}$ ) above the valence band edge ( $E_v$ ) in the P3HT MIS capacitors consisting of the different gate insulators, as determined by impedance spectroscopy.

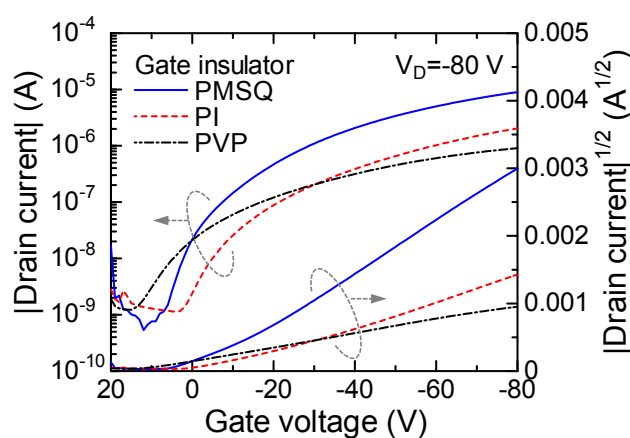


**Figure 9.** Transfer characteristics of bottom-gate/top-contact P3HT FETs with PMSQ, PI and PVP gate insulators measured at a drain voltage ( $V_D$ ) of  $-80\text{ V}$ .

**Table 2.** The field-effect mobility ( $\mu$ ) and the subthreshold slope (SS) of the bottom-gate/top-contact P3HT FETs with three different polymer gate insulators, together with the water contact angle (WCA) on polymer gate insulators.

Insulator	$\mu$ ( $\text{cm}^2\text{V}^{-1}\text{s}^{-1}$ )	SS (V/decade)	WCA (degree)
PMSQ	$1.0 \times 10^{-2}$	4.7	93
PI	$1.7 \times 10^{-3}$	7.3	80
PVP	$1.0 \times 10^{-4}$	9.3	64

#### 4. Conclusions

We have investigated the interface-state distributions in P3HT MIS capacitors with polymer gate insulators by using impedance spectroscopy. The effects of removing the peripheral regions, through the use of  $\text{O}_2$  plasma etching, and thermal annealing on the impedance characteristics of P3HT MIS

capacitors were demonstrated. It was found that the conductance characteristics of the P3HT MIS capacitors are in good agreement with the equivalent circuit model incorporating continuum interface states when the band-bending fluctuations are taken into consideration. We found that the determined interface-state distributions in P3HT MIS capacitors with PI, PVP, and PMSQ gate insulators are closely correlated with the electrical characteristics of P3HT FETs. The results indicate that polymer gate insulators having low-energy surfaces reduce the densities of the interface states in P3HT MIS devices as a result of the improvement of the crystallinity of P3HT films, leading to an improvement in the field-effect mobility and subthreshold characteristics.

**Author Contributions:** T.N., T.K., K.M., and H.N. were responsible for designing the project. Y.M. and H.H. contributed towards device fabrication and characterization. All authors discussed the results. T.N., H.H., and H.N. wrote and completed the manuscript.

**Funding:** This research was supported by Semiconductor Technology Academic Research Center (STARC), by a Grant-in-Aid for Scientific Research (B) (No. JP23360140) from the Japan Society for the Promotion of Science (JSPS), and by a Grant-in-Aid for Scientific Research on Innovative Areas “New Polymeric Materials Based on Element-Blocks (No. 2401)” (No. JP24102011) from the Ministry of Education, Culture, Sports, Science and Technology, Japan. This research was partially supported by a Grant-in-Aid for Scientific Research (B) (No. JP17H03238), by a Grant-in-Aid for Scientific Research (A) (No. JP17H01265) from JSPS, and by Support Center for Advanced Telecommunications (SCAT) Technology Research, Foundation, Japan.

**Acknowledgments:** We would like to thank Nissan Chemical Corporation for supplying polyimide.

**Conflicts of Interest:** The authors declare no conflict of interest.

## References

1. Sirringhaus, H. Organic field-effect transistors: The path beyond amorphous silicon. *Adv. Mater.* **2014**, *26*, 1319–1335. [[CrossRef](#)] [[PubMed](#)]
2. Klauk, H. Organic thin-film transistors. *Chem. Soc. Rev.* **2010**, *39*, 2643–2666. [[CrossRef](#)] [[PubMed](#)]
3. Veres, J.; Ogier, S.; Lloyd, G.; de Leeuw, D. Gate insulators in organic field-effect transistors. *Chem. Mater.* **2004**, *16*, 4543–4555. [[CrossRef](#)]
4. Kline, R.J.; McGehee, M.D.; Toney, M.F. Highly oriented crystals at the buried interface in polythiophene thin-film transistors. *Nat. Mater.* **2006**, *5*, 222–228. [[CrossRef](#)]
5. Jung, Y.; Kline, R.J.; Fischer, D.A.; Lin, E.K.; Heeney, M.; McCulloch, I.; DeLongchamp, D.M. The effect of interfacial roughness on the thin film morphology and charge transport of high-performance polythiophenes. *Adv. Funct. Mater.* **2008**, *18*, 742–750. [[CrossRef](#)]
6. Sheraw, C.D.; Gundlach, D.J.; Jackson, T.N. Spin-on polymer gate dielectric for high performance organic thin film transistors. *Mater. Res. Soc. Symp. Proc.* **2000**, *558*, 403–408. [[CrossRef](#)]
7. Sekitani, T.; Iba, S.; Kato, Y.; Someya, T. Bending effect of organic field-effect transistors with polyimide gate dielectric layers. *Jpn. J. Appl. Phys.* **2005**, *44*, 2841–2843. [[CrossRef](#)]
8. Klauk, H.; Halik, M.; Zschieschang, U.; Schmid, G.; Radlik, W.; Weber, W. High-mobility polymer gate dielectric pentacene thin film transistors. *J. Appl. Phys.* **2002**, *92*, 5259–5263. [[CrossRef](#)]
9. Bao, Z.; Kuck, V.; Rogers, J.A.; Paczkowski, M.A. Silsesquioxane resins as high-performance solution processible dielectric materials for organic transistor applications. *Adv. Funct. Mater.* **2002**, *12*, 526–531. [[CrossRef](#)]
10. Tomatsu, K.; Hamada, T.; Nagase, T.; Yamazaki, S.; Kobayashi, T.; Murakami, S.; Matsukawa, K.; Naito, H. Fabrication and characterization of poly(3-hexylthiophene)-based field-effect transistors with silsesquioxane gate insulators. *Jpn. J. Appl. Phys.* **2008**, *47*, 3196–3199. [[CrossRef](#)]
11. Nagase, T.; Hamada, T.; Tomatsu, K.; Yamazaki, S.; Kobayashi, T.; Murakami, S.; Matsukawa, K.; Naito, H. Low-temperature processable organic-inorganic hybrid gate dielectrics for solution-based organic field-effect transistors. *Adv. Mater.* **2010**, *22*, 4706–4710. [[CrossRef](#)] [[PubMed](#)]
12. Matsukawa, K.; Watanabe, M.; Hamada, T.; Nagase, T.; Naito, H. Polysilsesquioxanes for gate-insulating materials of organic thin-film transistors. *Int. J. Polym. Sci.* **2012**, *2012*, 852063. [[CrossRef](#)]
13. Meijer, E.J.; Mangnus, A.V.G.; Hart, C.M.; de Leeuw, D.M.; Klapwijk, T.M. Frequency behavior and the Mott–Schottky analysis in poly(3-hexyl thiophene) metal–insulator–semiconductor diodes. *Appl. Phys. Lett.* **2001**, *78*, 3902–3904. [[CrossRef](#)]

14. Torres, I.; Taylor, D.M.; Itoh, E. Interface states and depletion-induced threshold voltage instability in organic metal-insulator-semiconductor structures. *Appl. Phys. Lett.* **2004**, *85*, 314–316. [[CrossRef](#)]
15. Torres, I.; Taylor, D.M. Interface states in polymer metal-insulator-semiconductor devices. *J. Appl. Phys.* **2005**, *98*, 073710. [[CrossRef](#)]
16. Itoh, E.; Torres, I.; Taylor, D.M. The influence of interfacial charge exchange phenomena at the insulator-semiconductor interface on the electrical properties of poly(3-hexylthiophene) based field effect transistors. *Jpn. J. Appl. Phys.* **2005**, *44*, 641–647. [[CrossRef](#)]
17. Yun, M.; Gangopadhyay, S.; Bai, M.; Taub, H.; Arif, M.; Guha, S. Interface states in polyfluorene-based metal-insulator-semiconductor devices. *Org. Electron.* **2007**, *8*, 591–600. [[CrossRef](#)]
18. Alves, N.; Taylor, D.M. Determining the interfacial density of states in metal-insulator-semiconductor devices based on poly(3-hexylthiophene). *Appl. Phys. Lett.* **2008**, *92*, 103312. [[CrossRef](#)]
19. Nicollian, E.H.; Goetzberger, A. The Si-SiO<sub>2</sub> interface—Electrical properties as determined by the metal-insulator-silicon conductance technique. *Bell. Syst. Tech. J.* **1967**, *46*, 1055–1133. [[CrossRef](#)]
20. Nicollian, E.H.; Brews, J.R. *MOS (Metal Oxide Semiconductor) Physics and Technology*; Wiley Interscience: New York, NY, USA, 2003; ISBN 978-0-471-43079-7.
21. Noh, Y.-Y.; Kim, D.-Y.; Yase, K. Highly sensitive thin-film organic phototransistors: Effect of wavelength of light source on device performance. *J. Appl. Phys.* **2005**, *98*, 074505. [[CrossRef](#)]
22. Nicollian, E.H.; Goetzberger, A. Lateral AC current flow model for metal-insulator-semiconductor capacitors. *IEEE Trans. Electron. Devices* **1965**, *12*, 108–117. [[CrossRef](#)]
23. Itoh, E.; Torres, I.; Hayden, C.; Taylor, D.M. Excimer-laser micropatterned photobleaching as a means of isolating polymer electronic devices. *Synth. Met.* **2006**, *156*, 129–134. [[CrossRef](#)]
24. Jung, K.-D.; Lee, C.A.; Park, D.-W.; Park, B.-G.; Shin, H.; Lee, J.D. Admittance measurements on OFET channel and its modeling with R-C network. *IEEE Electron Device Lett.* **2007**, *28*, 204–206. [[CrossRef](#)]
25. Hoshino, S.; Yoshida, M.; Uemura, S.; Kodzasa, T.; Takada, N.; Kamata, T.; Yase, K. Influence of moisture on device characteristics of polythiophene-based field-effect transistors. *J. Appl. Phys.* **2004**, *95*, 5088–5093. [[CrossRef](#)]
26. Sze, S.M.; Ng, K.K. *Physics of Semiconductor Devices*, 3rd ed.; John Wiley & Sons, Inc.: New York, NY, USA, 2007; ISBN 978-0-471-14323-9.
27. Grecu, S.; Roggenbuck, M.; Opitz, A.; Brütting, W. Differences of interface and bulk transport properties in polymer field-effect devices. *Org. Electron.* **2006**, *7*, 276–286. [[CrossRef](#)]
28. Nicollian, E.H.; Goetzberger, A.; Lopez, A.D. Expedient method of obtaining interface state properties from MIS conductance measurements. *Solid-State Electron.* **1969**, *12*, 937–944. [[CrossRef](#)]
29. Simonne, J.J. A method to extract interface state parameters from the MIS parallel conductance technique. *Solid-State Electron.* **1973**, *16*, 121–124. [[CrossRef](#)]
30. Berglund, C.N. Surface states at steam-grown silicon-silicon dioxide interfaces. *IEEE Trans. Electron Devices* **1966**, *13*, 701–705. [[CrossRef](#)]
31. Shur, M.; Hack, M. Physics of amorphous silicon based alloy field-effect transistors. *J. Appl. Phys.* **1984**, *55*, 3831–3842. [[CrossRef](#)]



© 2018 by the authors. Licensee MDPI, Basel, Switzerland. This article is an open access article distributed under the terms and conditions of the Creative Commons Attribution (CC BY) license (<http://creativecommons.org/licenses/by/4.0/>).